THE JOURNAL OF PHYSICAL CHEMISTRY LETTERS
A JOURNAL OF THE AMERICAN CHEMICAL SOCIETY

pubs.acs.org/JPCL

Letter

Metallization of Quantum Material $GaTa_4Se_8$ at High Pressure

Hongshan Deng,* Jianbo Zhang, Min Yong Jeong, Dong Wang, Qingyang Hu, Shuai Zhang, Raimundas Sereika, Takeshi Nakagawa, Bijuan Chen, Xia Yin, Hong Xiao, Xinguo Hong, Jichang Ren, Myung Joon Han,* Jun Chang,* Hongming Weng, Yang Ding,* Hai-Qing Lin, and Ho-kwang Mao

Cite This: *J. Phys. Chem. Lett.* 2021, 12, 5601−5607

Read Online

HPSTR 1197-2021

ACCESS | Metrics & More | Article Recommendations | Supporting Information

ABSTRACT: Pressure is a unique thermodynamic variable to explore the phase competitions and novel phases inaccessible at ambient conditions. The resistive switching material $GaTa_4Se_8$ displays several quantum phases under pressure, such as a $J_{eff} = 3/2$ Mott insulator, a correlated quantum magnetic metal, and *d*-wave topological superconductivity, which has recently drawn considerable interest. Using high-pressure Raman spectroscopy, X-ray diffraction, extended X-ray absorption, transport measurements, and theoretical calculations, we reveal a complex phase diagram for $GaTa_4Se_8$ at pressures exceeding 50 GPa. In this previously unattained pressure regime, $GaTa_4Se_8$ ranges from a Mott insulator to a metallic phase and exhibits superconducting phases. In contrast to previous studies, we unveil a hidden correlation between the structural distortion and band gap prior to the insulator-to-metal transition, and the metallic phase shows superconductivity with structural and magnetic properties that are distinctive from the lower-pressure phase. These discoveries highlight that $GaTa_4Se_8$ is a unique material to probe novel quantum phases from a structural, metallicity, magnetism, and superconductivity perspective.

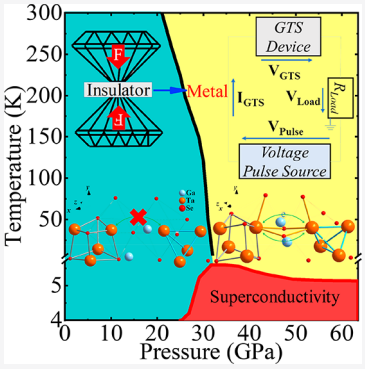

The quantum molecular $GaTa_4Se_8$ (GTS) is a candidate for resistive switching materials and memory devices, and it exhibits successive transitions from Mott insulator to metal and metal to superconductor[1] at high pressure. In addition to its unique magnetic and transport properties at ambient conditions, the phases that can arise in this material include intriguing topological *d*-wave superconductivity,[2] correlated $J_{eff} = 3/2$ metal,[3] spin-freezing superconductivity,[3] and a multipolar magnetic phase.[4] However, the vast, exciting possibilities remain largely unexplored, especially in the high-pressure regime.

GTS is commonly described as a deficient spinel with a symmetry of $F\bar{4}3m$. Tantalum atoms are shifted off the center of the Se octahedral cage, forming tetrahedral Ta_4Se_4 (or Ta_4) clusters with the intracluster Ta−Ta distances of <3 Å and the intercluster Ta−Ta distances of >4 Å. It remains in a cubic insulating phase to the lowest temperatures.[1,5,6] Previous high-pressure studies on GTS were carried out up to ∼26 GPa.[1] They revealed that GTS experienced an insulator-to-metal transition (IMT) at 17 GPa from a resistance measurement on polycrystalline samples,[1] 6 GPa from optical conductivity experiments on single crystals,[7] and 3.5 GPa from a resistance measurement on single crystals.[5] As no symmetry-breaking was reported during the IMT, this pressure-induced IMT has been regarded for decades as a Mott transition primarily driven by the electron−electron interaction.[1,5−14] In addition to the considerable divergence in reported IMT transition pressures, recent experiments[4] and theoretical results[15] also debate that possible structural changes are concurring with the IMT, which compel us to investigate the role of the GTS crystalline structures during the IMT transition and further explore the new quantum states in the higher-pressure regime.

To study how GTS's structure evolves with the IMT, a question still under considerable debate,[8,10,11,14] we have integrated the electrical resistance technique with Raman spectroscopy at high pressure for the simultaneous measurements of resistance and structural properties, which can effectively avoid the errors caused by different experimental conditions in individual measurements. Moreover, we recorded the pressure values every ∼20 K to disentangle the temperature effects on pressure (SM 1).

Figure 1a−h displays the results of the resistance measurements. From 0.8/5.0 GPa (300/7 K) (the term of "300/7 K" means the pressure of 0.8 GPa at 300 K increases to 5.0 GPa as temperature decreases to 7 K; this notation of 300/7 K is omitted at other pressures for simplicity) to 4.5/10.2 GPa, the resistance exhibits a temperature-dependent insulating behavior. From 4.5/10.2 GPa to 18.2/25.3 GPa, the resistance value drops by about 4 orders of magnitude. Though this phase is metal-like, having a much lower resistance than the Mott

Received: April 4, 2021
Accepted: May 27, 2021
Published: June 10, 2021

https://doi.org/10.1021/acs.jpclett.1c01069
J. Phys. Chem. Lett. 2021, 12, 5601−5607

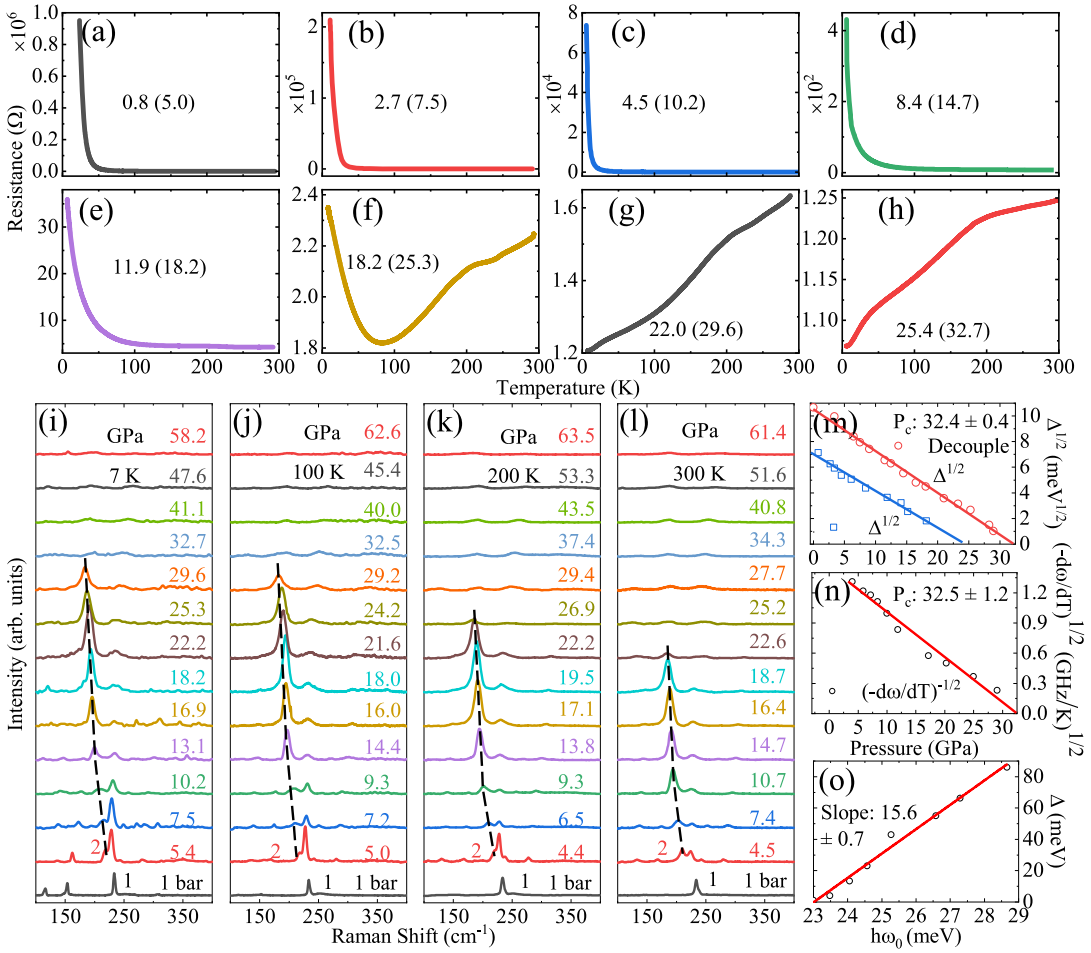

Figure 1. Results from electrical resistance and Raman measurements on $GaTa_4Se_8$ (GTS) at high pressure. Plots (a–h) show an IMT appears at 22.0/29.6 GPa (300/7 K). (i–l) The results of the Raman spectra were collected simultaneously with electrical resistance from 1 bar to 63.5 GPa and 300 to 7 K. The Raman peak at 200–250 cm^{-1} splits into peaks 1 and 2 immediately above ambient pressure. In contrast, peak 2 continuously softens with compression prior to the first-order structure transition occurring at 22.6/32.7 GPa. (m) The plot of linear fitting $\sqrt{\Delta}$ (in red) to pressure shows that Δ becomes zero at ∼32.4 (+0.4) GPa, yielding the value of P_c(IMT) at T = 0 k. In addition, the result (in blue) determined from the $P-T$ entangled data (pressure is only measured at 300 K) is also added for comparison. (n) The plot of linearly fitting $\sqrt{C}$ to pressure yields the P_c(s) = 32.50 (+1.2) GPa. (o) The correlation between Δ and $h\omega_0$ appears with a ratio of $\Delta/h\omega_0$ = 15.6.

insulating phase, it is still in an insulating phase due to its temperature dependence, showing an upturn at lower temperatures. The electronic state of the material under 18.2 /25.3 GPa appears to exhibit MIT-like behavior, which is the likelihood of phase separation or a possible magnetic "impurity" effect in this intermediate regime.

When the pressure reaches above 22.0/29.6 GPa, GTS turns into a metallic phase, in which the resistance decreases monotonically as the temperature is lowered (Figure 1g). Because the IMT pressure (P_c) increases from 22.0 GPa (300 K) to 29.6 GPa (7 K), there is no single pressure value corresponding to each $R-T$ curve due to the entanglement of temperature and pressure (SM 2). To solve this problem, the resistance data were selected with the same pressure from the two-dimensional map of $R(P,T)$ (SM 1), and the activation gap Δ (also equal to the band gap) was determined for each selected pressure point by fitting the data with the equation $\ln R(T) = \Delta/2k_BT$ (where k_B is the Boltzmann constant) (SM 1). It is noted that $\sqrt{\Delta}$ shows linearity with pressure, and it was determined the IMT $P_{c(IMT)}$ is ∼32.4 (±0.4) GPa at 0 K when Δ becomes 0 eV. In contrast, the conventional data analysis gives an IMT P_c' = 24.4 (±0.8) GPa at 0 K (blue line in Figure 1m), i.e., ∼8.0 GPa lower than the P_c determined from our new method (SM 2).

Accordingly, previous studies' inconsistency of the reported P_c is probably due to the values measured at room temperature, which are not the actual IMT P_c values (SM 2). Therefore, the comparison of these P_c values is not meaningful. Also, single crystals usually have anisotropic resistance[16−18] so that the IMT could occur at lower pressure along specific directions in single crystals than polycrystalline samples. This could be another source for the reported P_c values' inconsistency between single-crystal samples and polycrystalline samples.[19−22]

Parallel to the resistance measurements, the Raman spectra are simultaneously collected from the same sample at approximately every 50 K to monitor the possible change of structures. The Raman spectra are shown in Figure 1i–l, while more data are shown in (SM 3). The most notable change in Raman spectra is the splitting of the main peak into two peaks, i.e., peak 1 (∼250 cm^{-1}) and peak 2 (∼200 cm^{-1}), immediately above the ambient pressure, indicating a structural distortion (Figure 1i–l). Peak 1 corresponds to the vibration mode of the Ta_4Se_4 cluster.[1] The continuous softening of peak

https://doi.org/10.1021/acs.jpclett.1c01069
J. Phys. Chem. Lett. 2021, 12, 5601−5607

2 suggests the vibration mode of the distorted Ta_4Se_4 cluster becomes increasingly unstable at high pressure. However, such a distortion is too small to be distinguished in powder (SM 4) and single-crystal X-ray diffraction (XRD) (SM 5) and can only be detected in Raman spectra and extended X-ray absorption fine structure (EXAFS) spectra (see SM 4). Eventually, the Raman spectra show dramatic changes at 22.6/32.7 GPa, suggesting a first-order structure transition occurs. To conclusively and accurately determine if the structure transitions concur with IMT, we need to determine the structure transition pressure $P_{c(ST)}$ at 0 K and compare it with $P_{c(IMT)}$ at 0 K.

To this end, the $P_{c(ST)}$ at 0 K using $\frac{\partial^2\omega}{\partial T\partial P} = 0$ as a criterion (where ω is the frequency of peak 2) is determined, assuming the softening of peak 2 is a precursor of the first-order structure transition and ceases at the structure transition critical pressure. Similar to the determination of Δ, a two-dimensional map of $\omega(P,T)$ (peak 2) is constructed, and the ω values obtained at the same pressure are selected. By fitting ω to temperature with the equation $\omega = C*T + \omega_0$ (where ω_0 is the position of peak 2 at 0 K), C and ω_0 for each selected pressure point (SM 3) are obtained. $\sqrt{C}$ shows linearity with pressure, and it was determined the $P_{c(st)}$ is ∼32.5 (±1.2) GPa at 0 K when $\frac{d\sqrt{C}}{dP}$ becomes 0 ($\frac{\partial^2\omega}{\partial T\partial P}$ also becomes 0), as shown in Figure 1n. Within the uncertainties, $P_{c(ST)}$ appears identical to $P_{c(IMT)}$; it can thereby be concluded that the IMT and the first-order structure transition indeed concur at ∼32.4 GPa and 0 K. More intriguingly, prior to the IMT and the first-order structure transition occurring, ω_0 and Δ show persisting linearity with a ratio of $\frac{d\Delta}{d\omega_0} = 15.6$, (Figure 1o). This result provides compelling evidence of a correlation between the structural distortion and band gap, which was not elucidated by previous studies.

These findings suggest that the current understanding of IMT in the GTS material requires an update: the role of pressure is not only to increase the intercluster hopping and thus to reduce the U/t value of the Hubbard model[12−15,20] but also to expand the bandwidth by removing part of the orbital degeneracy to assist the Mott transition, being similar to the well-known Mott−Peierls type IMT in VO_2.[23−27] However, the IMT in VO_2 results in a metallic phase with a higher symmetry than its insulating phase. In contrast, the IMT in GTS leads to a metallic phase with a lower symmetry than its insulating phase, implying that the driving force of the IMTs in these two material systems may be different, so further experimental and theoretical investigations are required.

To further characterize the metallic phase's crystal structure after the IMT, a separate high-pressure powder X-ray diffraction experiment on polycrystalline GTS samples was performed. The results displayed in Figure 2a show no appreciable structural distortion could be identified from XRD patterns up to ∼23.4 GPa at 300 K, consistent with previous reports.[1,6] A new peak appears at P = 23.4 GPa (300 K; indicated by an arrow) to evidence the emergence of a first-order structure transition. The transition pressure is roughly consistent with the IMT pressure of 22.0 GPa at 300 K. The structure determination and refinement based on the diffraction patterns indicate the new metallic phase has a $C2$ symmetry that inherits the similar Ta_4Se_4 clusters' basic molecular unit and the cubic phase's topological configurations (as shown in Figure 2c,d). However, it has a reduced

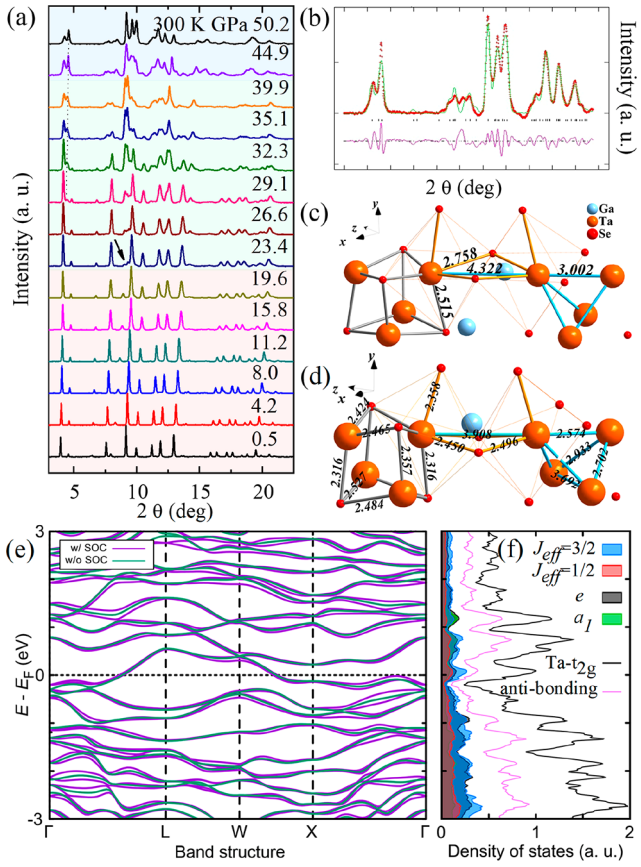

Figure 2. Diffraction patterns displayed in (a) are collected at 300 K, where a structure transition appears above 23.4 GPa. The new high-pressure phase continuously evolves with pressure and eventually becomes stable above 39.9 GPa. (b) The Rietveld refinement result of the X-ray diffraction pattern for 50.2 GPa. (c) The structure models are the results of ambient pressure and the following atomic positions: Ga 4a (0, 0, 0), Ta 16e (0.6024, 0.6024, 0.6024), Se1 16e (0.3643, 0.3643, 0.3643), Se2 16e (0.8646, 0.8646, 0.8646). (d) The structure models are the results of 50.2 GPa and the following atomic positions: Ga 2a (−1, −0.9338, 0), Ta1 4c (0.0829, −0.6193, 1.3179), Ta2 4c (−0.1972, −0.3895, 0.8234), Se1 4c (−0.0537, −0.3026, 0.6886), Se2 4c (0.2348, −0.6985, 1.1774), Se3 4c (−0.0149, −0.9378, 1.6781), Se4 4c (−0.7, −0.0853, 0.2503). (e) The calculated band structure of the metal phase. The violet and green lines represent the results with and without spin orbit coupling (SOC), respectively. (f) The projected DOS for the metal phase around the Fermi level. Gray-, green-, blue-, and red-shaded regions represent the projected DOS onto the bonding orbitals of the molecular e, a_1, J_{eff} = 3/2, and J_{eff} = 1/2 states, respectively. The molecular orbital nature is no longer well-retained in this high-pressure regime. The black and magenta solid lines refer to the Ta-t_{2g} and the antibonding orbital state, respectively.

intercluster distance and a more distorted Ta_4Se_4 cluster (see SM 6). This symmetry change in the crystal structure has not been reported in previous studies.[1,5−7]

Additional density functional theory (DFT) calculations were done to investigate the new metallic phase's electronic structure with the same schemes applied in refs 12 and 28. Figure 2e,f shows the band dispersion and the density of states (DOS), respectively, calculated with the structure obtained experimentally at $P \approx$ 50.2 GPa. GTS exhibits a metallic character, and the electronic structure does not significantly change by including SOC. Moreover, the molecular orbitals are not well-defined, and the projection onto the J_{eff} state fails, implying that GTS's molecular nature is no longer retained; we

https://doi.org/10.1021/acs.jpclett.1c01069
J. Phys. Chem. Lett. 2021, 12, 5601−5607

also find that the metal phase is nonmagnetic, as its ground state is far from the magnetic stability (SM 7). Therefore, the metal phase is different from the low-pressure insulting phase for which the well-defined J_{eff} = 3/2 moment is revealed by previous RIXS experiment, and DFT + U and DFT + DMFT calculations.[2,12,28]

In the study of IMT, the temperature can only be lowered to 6−7 K, not enough to study the superconductivity in GTS that is reported to start near 5 K.[1] Thus, the second round of resistance measurements was performed using a physical property measurement system (PPMS) to extend the study of superconductivity up to 50.3 GPa. In this study, the temperature could be lowered to ∼2 K, and the results are displayed in Figure 3a−e. The superconductivity appears

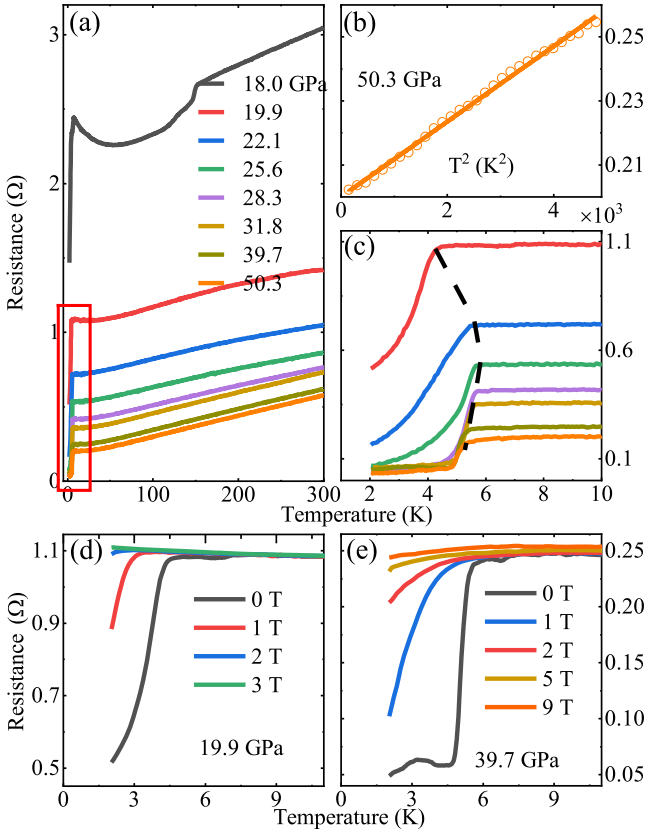

Figure 3. Superconductivity and pressure−temperature phase diagram of $GaTa_4Se_8$. (a) The high-pressure resistance measurements of GTS up to 50.3/57.3 GPa (300/2 K). (b) The Fermi liquid fitting of resistance vs T^2 from 10 to 70 K at 50.3/57.3 GPa (300/2 K). (c) The plot of superconductivity is measured at high pressure. (d,e) shows the temperature dependence of resistance under different magnetic fields up to 3 T at 19.9/26.9 GPa (300/2 K) and up to 9 T at 39.7/46.7 GPa (300/2 K), respectively.

around 18.0/25.0 GPa (300/2 K) (SM 8) with a T_c of ∼3.95 K in the semiconductor phase. This result is roughly consistent with the previous report.[1] Moreover, it again indicates that GTS turns into a complete metallic phase at ∼22.1/29.1 GPa (300/2 K), consistent with the results from first-round measurements. The superconductivity is maintained at 50.3/57.3 GPa (300/2K) (the maximum pressure achieved). T_c increases to 5.6 K once GTS enters a metallic phase at ∼19/29 GPa (300/2 K) and decreases slightly with pressure up to 50.3/57.3 GPa (300/2 K). There is no indication of a strong departure from Fermi liquid behavior, since the parameter n remains at 2 in the equation $R = R_0 + a*T^n$, below 70 K (Figure 3b). The critical field is about 3 T at 19.9/26.6 GPa with a T_c of ∼4 K (Figure 3d), but it becomes more than 9 T at ∼50.3/57.3 GPa (300/2 K) (Figure 3e).

A previous theoretical study[2] suggests topological d-wave superconductivity based on the molecular J_{eff} = 3/2 band structure in the relatively low-pressure regime. The calculation shows that the electronic band structure's molecular nature breaks down under high enough pressure, and the material turns out to be a usual atomic solid. As discussed above and supported by the transport data, this high-pressure phase is close to Fermi liquid. Thus, the situation seems to imply the possibility that there is a conventional Bardeen−Cooper−Schrieffer (BCS)-type superconductivity residing in a high-pressure metallic phase, which is distinctive from that at lower pressure. This conjecture seems consistent with the fact that the observed superconductivity shows a maximum T_c at IMT, which does not exhibit the usual pressure-dependent dome shape but extends up to the highest pressure without a rapidly decreasing T_c. This possibility deserves further investigation.

In conclusion, our results establish GTS as a unique material system in which the Mott insulator, correlated J_{eff} = 3/2 metal,[29] and conventional metal phase successively arise as a function of pressure. To summarize, Figure 4a displays the constructed $P-T$ phase diagram. It is observed that the Mott insulator-to-metal transition concurs with a symmetry-lowering structural transition from cubic to monoclinic, renewing our understanding of IMT in this material at high pressure. The superconducting state appears in the insulating state and close to Fermi liquid metallic state up to 50.3 GPa, which is possibly

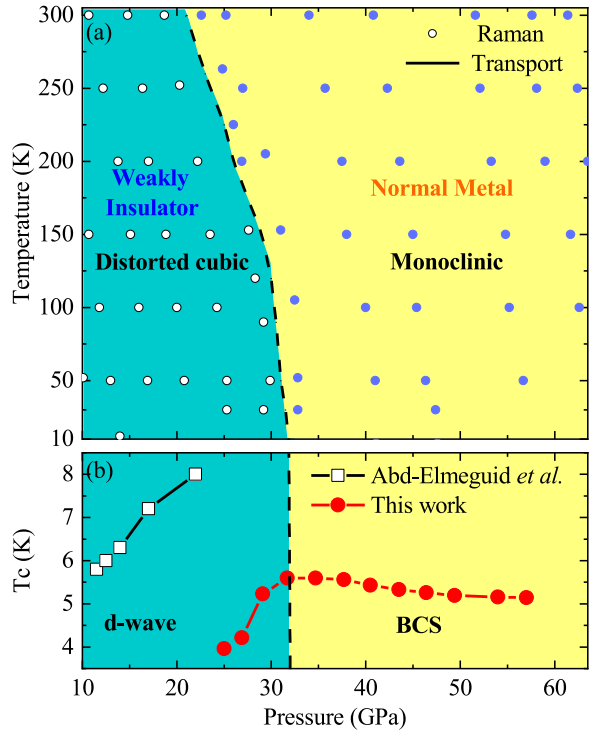

Figure 4. Pressure−temperature phase diagram of $GaTa_4Se_8$. (a) The phase diagram of GTS. Transport measurements and Raman measurements define the phase boundary. (b) Superconductivity T_c evolution with the pressure of GTS. The black line is reported by Abd-Elmeguid et al.[1] The red line is obtained from Figure 3b.

https://doi.org/10.1021/acs.jpclett.1c01069
J. Phys. Chem. Lett. 2021, 12, 5601−5607

a BCS-type superconductor distinct from the *d*-wave type one reported in the low-pressure regime.

EXPERIMENTAL SECTION

Sample Preparation and Characterization. Polycrystalline and single-crystal samples of GTS were prepared by the selenium transport method as described in ref 6. The GTS powders were then placed in an evacuated silica tube with a slight excess of, heated at 950 °C for 24 h, and then slowly cooled down (2 °C h^{-1}) to room temperature to avoid the vacancy of elemental selenium. The sample was characterized by X-ray diffraction at HPCAT 16-BM-D, Advanced Photon Source, Argonne National Lab. Powder diffraction patterns were well-indexed using the previously reported crystal structural data.[1,6,7]

High-Pressure Electrical Measurements. The electronic transport properties under high pressure and low temperature were investigated via the van der Pauw electrical conductivity method in a CuBe alloy symmetric diamond anvil cell (DAC). The pressure was generated by a pair of diamonds with a 400 μm diameter culet. A gasket made of stainless steel was pressed, and a hole was drilled into the center of the gasket with a diameter of the diamond culet. A cubic boron nitride (c-BN)-epoxy insulation layer was prepared to protect the electrode leads from the metallic gasket. Finally, a hole with a 280 μm diameter was drilled in the center of the c-BN gasket. The NaCl powder was used as the pressure-transmitting medium. Four platinum strips were arranged to contact the sample in the chamber. The first-round experiments at different pressure−temperature conditions were performed using a laboratory-designed (with optical window) electrical transport system where a Keithley 6221 current source, 2182A nanovolt meter, and 7001 switch device were used as the current supply, voltmeter, and voltage/current switcher, respectively. The pressure was measured via the ruby fluorescence method at every ∼20 K (from 5 to 300 K). The second-round high-pressure electrical transport experiments were conducted using the Quantum Design physical property measurement system by 23 mm-type CuBe cells.

High-Pressure Raman Spectroscopy. Raman spectra were recorded in backscattering geometry using a microspectrometer with the symmetric cell. The DAC had a pair of ultralow fluorescence type II diamonds with a 300 μm culet size and was set in a microscopy cryostat system (Cryo Industries of America, Inc.) with a T301 steel gasket. The silicon diode sensor bought from Cryogenic Control Systems, Inc. was used for 7−300 K temperature calibration. A micro-Raman system (Renishaw, UK) with a 533 nm laser excitation was applied to obtain the sample's Raman spectra. A grating of 2400 grooves/mm was employed throughout the experiment, and the laser beam spot was about 20−30 μm. The ruby fluorescence was used to calibrate the pressure with Ne as the pressure medium.

High-Pressure X-ray Powder Diffraction. The pressure dependence of the lattice constants of GTS powder samples was measured at room temperature up to about 8 GPa by angular dispersive X-ray diffraction (ADXRD) at HPCAT 16-BM-D using the symmetric DAC with Boehler-type diamonds and a T301 stainless steel gasket. Ne was loaded as the pressure-transmitting medium to maintain good hydrostatic pressure. The incident X-ray beam size was ∼10 μm with an energy of 40 keV. The flow cryostat was applied to conduct the low-temperature diffraction down to 30 K. A Mar345 CCD was used as the detector. An online ruby system was employed to measure the ruby fluorescence signal for pressure determination. The imaged diffraction was integrated using the DIOPTAS software to acquire the diffraction intensity vs 2θ data sets. Crystallographic parameters and structure simulation were analyzed by Rietveld full-profile refinement using the General Structure Analysis System (GSAS) program.[30]

High-Pressure X-ray Single-Crystal Diffraction. The high-pressure X-ray single-crystal diffraction measurements were carried out on GTS up to 30 GPa at room temperature using the Bruker D8 Quest diffractometer equipped with Mo Kα radiation. Data were collected with an Sc-type cell with an X-ray window opening of 20 degrees. The data reduction,[31] structure solution,[32] and refinement[33] were conducted with program APEX3.

First-Principles Calculations. The electronic structure calculations based on density functional theory (DFT) were carried out using the "OpenMX" code, which is based on the linear combination of pseudoatomic orbitals.[34] Local density approximation (LDA)[35,36] was used for the exchange-correlation functional. A cutoff energy of 400 Ry and a 12 × 12 × 12 Monkhorst-pack grid for momentum-space integration were adopted. The SOC was treated within the fully relativistic j-dependent pseudopotential and noncollinear scheme.[37] The primitive unit cell of the experimentally determined *C*2 monoclinic structure was used for our calculations.

ASSOCIATED CONTENT

Supporting Information

The Supporting Information is available free of charge at https://pubs.acs.org/doi/10.1021/acs.jpclett.1c01069.

Detailed disentangle method, entangle activation energy, low-pressure structure, single-crystal diffraction analysis, crystal structure details, metal phase details (PDF)

AUTHOR INFORMATION

Corresponding Authors

Hongshan Deng − *Center for High Pressure Science and Technology Advanced Research, Beijing 100094, People's Republic of China*; orcid.org/0000-0002-6871-2739; Email: hongshan.deng@hpstar.ac.cn

Myung Joon Han − *Department of Physics, Korea Advanced Institute of Science and Technology, Daejeon 34141, Korea*; orcid.org/0000-0002-8089-7991; Email: mj.han@kaist.ac.kr

Jun Chang − *College of Physics and Information Technology, Shaanxi Normal University, Xi'an 710119, People's Republic of China*; Email: junchang@snnu.edu.cn

Yang Ding − *Center for High Pressure Science and Technology Advanced Research, Beijing 100094, People's Republic of China*; Email: yang.ding@hpstar.ac.cn

Authors

Jianbo Zhang − *Center for High Pressure Science and Technology Advanced Research, Beijing 100094, People's Republic of China*; orcid.org/0000-0002-8339-1099

Min Yong Jeong − *Department of Physics, Korea Advanced Institute of Science and Technology, Daejeon 34141, Korea*

Dong Wang − *Center for High Pressure Science and Technology Advanced Research, Beijing 100094, People's Republic of China*; orcid.org/0000-0001-5004-9732

https://doi.org/10.1021/acs.jpclett.1c01069
J. Phys. Chem. Lett. 2021, 12, 5601−5607

Qingyang Hu − *Center for High Pressure Science and Technology Advanced Research, Beijing 100094, People's Republic of China;* orcid.org/0000-0002-2742-3017
Shuai Zhang − *Beijing National Laboratory for Condensed Matter Physics, and Institute of Physics, Chinese Academy of Sciences, Beijing 100190, People's Republic of China*
Raimundas Sereika − *Center for High Pressure Science and Technology Advanced Research, Beijing 100094, People's Republic of China;* orcid.org/0000-0001-5365-6773
Takeshi Nakagawa − *Center for High Pressure Science and Technology Advanced Research, Beijing 100094, People's Republic of China*
Bijuan Chen − *Center for High Pressure Science and Technology Advanced Research, Beijing 100094, People's Republic of China*
Xia Yin − *Center for High Pressure Science and Technology Advanced Research, Beijing 100094, People's Republic of China*
Hong Xiao − *Center for High Pressure Science and Technology Advanced Research, Beijing 100094, People's Republic of China;* orcid.org/0000-0001-8859-9967
Xinguo Hong − *Center for High Pressure Science and Technology Advanced Research, Beijing 100094, People's Republic of China*
Jichang Ren − *Nano and Heterogeneous Materials Center, School of Materials Science and Engineering, Nanjing University of Science and Technology, Nanjing 210094, People's Republic of China*
Hongming Weng − *Beijing National Laboratory for Condensed Matter Physics, and Institute of Physics, Chinese Academy of Sciences, Beijing 100190, People's Republic of China;* orcid.org/0000-0001-8021-9413
Hai-Qing Lin − *Beijing Computational Science Research Center, Beijing 100084, People's Republic of China*
Ho-kwang Mao − *Center for High Pressure Science and Technology Advanced Research, Beijing 100094, People's Republic of China*

Complete contact information is available at: https://pubs.acs.org/10.1021/acs.jpclett.1c01069

Author Contributions

All authors have given approval to the final version of the manuscript.

Funding

Y.D. is grateful for support from the National Key Research and Development Program of China 2018YFA0305703, Science Challenge Project, No TZ2016001, and the National Natural Science Foundation of China (NSFC): U1930401, 11874075. M.Y.J. and M.J.H. were supported by the Basic Science Research Program (2018R1A2B2005204) by the Creative Materials Discovery Program through NRF (2018M3D1A1058754) funded by the Ministry of Science and ICT (MSIT) of Korea and by the KAIST Grand Challenge 30 Project (KC30) in 2019 funded by the MSIT of Korea and KAIST. Q.H. is supported by the CAEP Research Project (CX20210048) a Tencent Xplorer prize.

Notes

The authors declare no competing financial interest.

■ ACKNOWLEDGMENTS

We acknowledge sectors 16 BM-D of the Advanced Photon Source, a U.S. Department of Energy (DOE) Office of Science user facility operated by Argonne National Laboratory (ANL) that is supported by the U.S. DOE Award No. DE-AC02-06CH11357, and beamline U2A of the National Synchrotron Light Source (NSLS), Brookhaven National Laboratory. The electric transport and Raman spectroscopy measurements were performed at the Center for High-Pressure Science & Technology Advanced Research. The authors thank S. Tkachev for help with the gas loading at the Advanced Photon Source. We thank LetPub (www.letpub.com) for its linguistic assistance during the preparation of this manuscript.

■ REFERENCES

(1) Abd-Elmeguid, M. M.; Ni, B.; Khomskii, D. I.; Pocha, R.; Johrendt, D.; Wang, X.; Syassen, K. Transition from Mott insulator to superconductor in $GaNb_4Se_8$ and $GaTa_4Se_8$ under high pressure. *Phys. Rev. Lett.* **2004**, *93* (12), 126403.
(2) Park, M. J.; Sim, G.; Jeong, M. Y.; Mishra, A.; Han, M. J.; Lee, S. Pressure-induced topological superconductivity in the spin−orbit Mott insulator $GaTa_4Se_8$. *npj Quantum Mater.* **2020**, *5* (1), 41.
(3) Jeong, M. Y.; Chang, S. Y.; Lee, H. J.; Sim, J.-H.; Lee, K. J.; Janod, E.; Cario, L.; Said, A.; Bi, W.; Werner, P.; Go, A.; Kim, J.; Han, M. J. J_{eff} = 3/2 metallic phase and unconventional superconductivity in $GaTa_4Se_8$. *Phys. Rev. B* **2021**, *103* (8), L081112.
(4) Ishikawa, H.; Yajima, T.; Matsuo, A.; Ihara, Y.; Kindo, K. Nonmagnetic ground states and a possible quadrupolar phase in 4d and 5d lacunar spinel selenides GaM_4Se_8 (M= Nb, Ta). *Phys. Rev. Lett.* **2020**, *124* (22), 227202.
(5) Camjayi, A.; Acha, C.; Weht, R.; Rodriguez, M. G.; Corraze, B.; Janod, E.; Cario, L.; Rozenberg, M. J. First-order insulator-to-metal Mott transition in the paramagnetic 3D system $GaTa_4Se_8$. *Phys. Rev. Lett.* **2014**, *113* (8), 086404.
(6) Pocha, R.; Johrendt, D.; Ni, B.; Abd-Elmeguid, M. M. Crystal structures, electronic properties, and pressure-induced superconductivity of the tetrahedral cluster compounds $GaNb_4S_8$, $GaNb_4Se_8$, and $GaTa_4Se_8$. *J. Am. Chem. Soc.* **2005**, *127*, 8732−8740.
(7) Ta Phuoc, V.; Vaju, C.; Corraze, B.; Sopracase, R.; Perucchi, A.; Marini, C.; Postorino, P.; Chligui, M.; Lupi, S.; Janod, E.; Cario, L. Optical conductivity measurements of $GaTa_4Se_8$ under high pressure: evidence of a bandwidth-controlled insulator-to-metal Mott transition. *Phys. Rev. Lett.* **2013**, *110* (3), 037401.
(8) Cario, L.; Vaju, C.; Corraze, B.; Guiot, V.; Janod, E. Electric-field-induced resistive switching in a family of Mott insulators: Towards a new class of RRAM memories. *Adv. Mater.* **2010**, *22* (45), 5193−5197.
(9) Dubost, V.; Cren, T.; Vaju, C.; Cario, L.; Corraze, B.; Janod, E.; Debontridder, F.; Roditchev, D. Resistive switching at the nanoscale in the Mott insulator compound $GaTa_4Se_8$. *Nano Lett.* **2013**, *13* (8), 3648−3653.
(10) Guiot, V.; Cario, L.; Janod, E.; Corraze, B.; Ta Phuoc, V.; Rozenberg, M.; Stoliar, P.; Cren, T.; Roditchev, D. Avalanche breakdown in $GaTa_4Se_{8-x}Te_x$ narrow-gap Mott insulators. *Nat. Commun.* **2013**, *4*, 1722.
(11) Guiot, V.; Janod, E.; Corraze, B.; Cario, L. Control of the electronic properties and resistive switching in the new series of Mott insulators $GaTa_4Se_{8-y}Te_y$ ($0 \le y \le 6.5$). *Chem. Mater.* **2011**, *23* (10), 2611−2618.
(12) Jeong, M. Y.; Chang, S. H.; Kim, B. H.; Sim, J. H.; Said, A.; Casa, D.; Gog, T.; Janod, E.; Cario, L.; Yunoki, S.; Han, M. J.; Kim, J. Direct experimental observation of the molecular Jeff = 3/2 ground state in the lacunar spinel $GaTa_4Se_8$. *Nat. Commun.* **2017**, *8* (1), 782.
(13) Stoliar, P.; Cario, L.; Janod, E.; Corraze, B.; Guillot-Deudon, C.; Salmon-Bourmand, S.; Guiot, V.; Tranchant, J.; Rozenberg, M. Universal electric-field-driven resistive transition in narrow-gap Mott insulators. *Adv. Mater.* **2013**, *25* (23), 3222−3226.
(14) Vaju, C.; Cario, L.; Corraze, B.; Janod, E.; Dubost, V.; Cren, T.; Roditchev, D.; Braithwaite, D.; Chauvet, O. Electric-pulse-driven electronic phase separation, insulator-metal transition, and possible

superconductivity in a Mott insulator. *Adv. Mater.* **2008**, *20*, 2760−2765.
(15) Zhang, S.; Zhang, T.; Deng, H.; Ding, Y.; Chen, Y.; Weng, H. Crystal and electronic structure of $GaTa_4Se_8$ from first-principles calculations. *Phys. Rev. B: Condens. Matter Mater. Phys.* **2020**, *102* (21), 214114.
(16) Tozer, S. W.; Kleinsasser, A. W.; Penney, T.; Kaiser, D.; Holtzberg, F. Measurement of anisotropic resistivity and Hall constant for single-crystal $YBa_2Cu_3O_{7-x}$. *Phys. Rev. Lett.* **1987**, *59* (15), 1768−1771.
(17) Worthington, T. K.; Gallagher, W. J.; Dinger, T. R. Anisotropic nature of high-temperature superconductivity in single-crystal $Y_1Ba_2Cu_3O_{7-x}$. *Phys. Rev. Lett.* **1987**, *59* (10), 1160−1163.
(18) Hidaka, Y.; Enomoto, Y.; Suzuki, M.; Oda, M.; Katsui, A.; Murakami, T. Anisotropy of the Upper Critical Magnetic Field in Single Crystal $YBa_2Cu_3O_{7+y}$. *Jpn. J. Appl. Phys., Part 2* **1987**, *26* (5), L726.
(19) Nakamura, Y.; Uchida, S. Anisotropic transport properties of single-crystal $La_{2-x}Sr_xCuO_4$: Evidence for the dimensional crossover. *Phys. Rev. B: Condens. Matter Mater. Phys.* **1993**, *47* (13), 8369−8372.
(20) Adachi, T.; Tanaka, H.; Kobayashi, H.; Miyazaki, T. Electrical resistivity measurements on fragile organic single crystals in the diamond anvil cell. *Rev. Sci. Instrum.* **2001**, *72* (5), 2358−2360.
(21) Ding, Y.; Yang, L.; Chen, C. C.; Kim, H. S.; Han, M. J.; Luo, W.; Feng, Z.; Upton, M.; Casa, D.; Kim, J.; et al. Pressure-Induced Confined Metal from the Mott Insulator $Sr_3Ir_2O_7$. *Phys. Rev. Lett.* **2016**, *116* (21), 216402.
(22) Kastner, M. A.; Birgeneau, R. J.; Shirane, G.; Endoh, Y. Magnetic, transport, and optical properties of monolayer copper oxides. *Rev. Mod. Phys.* **1998**, *70* (3), 897−928.
(23) Kim, H. T.; Lee, Y. W.; Kim, B. J.; Chae, B. G.; Yun, S. J.; Kang, K. Y.; Han, K. J.; Yee, K. J.; Lim, Y. S. Monoclinic and correlated metal phase in VO_2 as evidence of the Mott transition: Coherent Phonon analysis. *Phys. Rev. Lett.* **2006**, *97* (26), 266401.
(24) Yuan, X.; Zhang, Y.; Abtew, T. A.; Zhang, P.; Zhang, W. VO_2: Orbital competition, magnetism, and phase stability. *Phys. Rev. B: Condens. Matter Mater. Phys.* **2012**, *86*, 235103.
(25) Yuan, X.; Zhang, W.; Zhang, P. Hole-lattice coupling and photo-induced insulator-metal transition in VO_2. *Phys. Rev. B: Condens. Matter Mater. Phys.* **2013**, *88*, 035119.
(26) Zhu, Z.; Schwingenschloegl, U. Comprehensive picture of VO_2 from band theory. *Phys. Rev. B: Condens. Matter Mater. Phys.* **2012**, *86* (7), 075149.
(27) Kim, S.; Kim, K.; Kang, C.-J.; Min, B. I. Correlation-assisted phonon softening and the orbital-selective Peierls transition in VO_2. *Phys. Rev. B: Condens. Matter Mater. Phys.* **2013**, *87*, 195106.
(28) Kim, H.-S.; Im, J.; Han, M. J.; Jin, H. Spin-orbital entangled molecular Jeff states in lacunar spinel compounds. *Nat. Commun.* **2014**, *5*, 3988.
(29) Jeong, M. Y.; Chang, S. H.; Lee, H. J.; Sim, J.-H.; Lee, K. J.; Janod, E.; Cario, L.; Said, A.; Bi, W.; Werner, P.; Go, A.; Kim, J.; Han, M. J. Jeff = 3/2 metallic phase and unconventional superconductivity in $GaTa_4Se_8$. *Phys. Rev. B: Condens. Matter Mater. Phys.* **2021**, *103* (8), L081112.
(30) Toby, B. H.; Von Dreele, R. B. GSAS-II: the genesis of a modern open-source all purpose crystallography software package. *J. Appl. Crystallogr.* **2013**, *46* (2), 544−549.
(31) Bruker. *APEX2, SAINT, and SADABS*; Bruker AXS Inc.: Madison, Wisconsin, 2009.
(32) Sheldrick, G. M. SHELXT − Integrated space-group and crystal-structure determination. *Acta Crystallogr., Sect. A: Found. Adv.* **2015**, *71* (1), 3−8.
(33) Sheldrick, G. M. Crystal structure refinement with SHELXL. *Acta Crystallogr., Sect. C: Struct. Chem.* **2015**, *71* (1), 3−8.
(34) Ozaki, T. Variationally optimized atomic orbitals for large-scale electronic structures. *Phys. Rev. B: Condens. Matter Mater. Phys.* **2003**, *67*, 155108.
(35) Ceperley, D. M.; Alder, B. J. Ground state of the electron gas by a stochastic method. *Phys. Rev. Lett.* **1980**, *45* (7), 566−569.
(36) Perdew, J. P.; Zunger, A. Self-interaction correction to density-functional approximations for many-electron systems. *Phys. Rev. B: Condens. Matter Mater. Phys.* **1981**, *23*, 5048−5079.
(37) Macdonald, A. H. Spin-polarised relativistic exchange energies and potentials. *J. Phys. C: Solid State Phys.* **1983**, *16* (20), 3869−3876.

https://doi.org/10.1021/acs.jpclett.1c01069
J. Phys. Chem. Lett. 2021, 12, 5601−5607